Proceedings of the ASME 2021 16th International Manufacturing Science and Engineering Conference
MSEC2021
June 21-25, 2021, Virtual, Online

MSEC2021-63803

CHARACTERIZING THE CONDUCTIVITY OF AEROSOL JET PRINTED SILVER FEATURES ON GLASS

Dilan Ratnayake, Alexander Thomas Curry, Chuang Qu, John Usher, Kevin Walsh
University of Louisville
Louisville, KY

ABSTRACT

Aerosol Jet Printing is a promising technology for expanding fields such as printable electronics. It is compatible with a wide range of inks and can be printed on nearly any type of surface topology due to its 3-5 mm standoff distance from the substrate. However, nearly all printed inks require some form of post-sintering processing to achieve reasonable electrical conductivity. While several companies manufacture inks for aerosol jet printing, they only provide a narrow range of post processing results to demonstrate the achievable conductivity data. In this paper, a design of experiment (DOE) strategy using Van der Pauw printed pads is presented which can be applied to characterizing any conductive ink. We focus on a silver nano-particle ink from Clariant and monitor its conductivity under various thermal curing conditions, including temperature and time. From these results, a linear regression model is used to develop an equation that predicts the expected conductivity of the printed ink over a relatively-wide "time-temperature" design space. Such a characterization process and predictive equation are extremely useful for applications involving limited or restricted thermal budgets, such as flexible electronics.

Keywords: Aerosol Jet Printing, Optomec, sintering, conductivity, DOE, Van der Pauw

NOMENCLATURE

ρ	resistivity
σ	conductivity
h	thickness
t	time
T	temperature
I	supply current
V	sensed voltage

1. INTRODUCTION

The concept of Aerosol Jet Printing (AJP) was developed by a Mesoscale Integrated Conformal Electronics (MICE) project that was funded by the Defense Advanced Research Projects Agency (DARPA) in the 1990s [1]. The goal of this funded project was to develop a process capable of conformally depositing a wide range of materials on nearly any substrate. AJP is now commercialized by Optomec, Inc., who hold several patents for their AJP process [2]. A typical AJP system consists of two major components (atomizing the raw materials and depositing focused material), as shown in Figure 1. AJP works by placing ink into either an ultrasonic or pneumatic atomizer that turns the liquid ink into a dense mist. The mist is routed to the deposition head where it becomes focused by a controlled sheath gas, usually Nitrogen. As the aerosol stream and gas pass through the nozzle, they form a tight beam and accelerate. This high velocity stream remains in tight formation from the nozzle all the way to the substrate, which is typically 2-5 mm away from the nozzle [3]. The AJP process can print features as small as 10 microns all the way up to over a millimeter [4, 5]. This is achieved by utilizing different nozzle sizes.

AJP has an extremely wide range of printable materials. Metals such as gold, platinum, silver, and copper can be made into inks as well as polymers such as polyimide, PEDOT, and SU-8 just to name a few [6]. AJP can also print semiconductor materials, resistors, dielectrics/insulators, carbon, resists, and even carbon nanotubes. Any substance that can be manufactured into some form of ink is most likely compatible with the AJP process. Typically, any ink that has a viscosity between 1-1000 cP is printable, although this range of values changes depending on the type of atomization used. The quality and composition of the ink is very important to the final morphology and characteristics of the material after printing. Most materials also require some form of post processing to finalize their properties.

Post processing is usually done by sintering the material in the oven [7], curing with Intense Pulse Light [8], or sintering with a laser over the same contours printed. Some materials can also be cured by UV light, although most printable metals do not fall into this category.

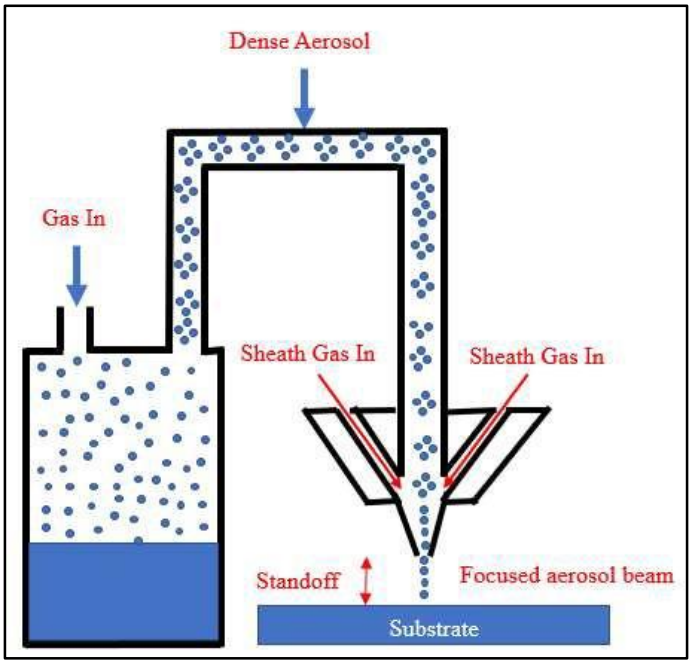

FIGURE 1: SCHEMATIC OF THE AEROSOL JET PROCESS.

2. MATERIALS AND METHODS

This study used an Aerosol Jet Print Engine with a Decathlon Print Cassette from Optomec for all printing processes. An ultrasonic atomizer was used to atomize a silver ink made by Clariant. After printing, the silver ink was cured in an oven in ambient conditions. The focus of this study was to characterize the response of the Clariant silver ink in the oven with varying time and temperature and measure the resulting conductivity. Using these results, a statistical model was developed to show how the conductivity changed with time and temperature using a linear regression model.

2.1 Optomec Aerosol Print Engine System

The Optomec aerosol print engine was used to study the conductivity of printed features on the glass wafers. The current system consists of a print engine, a process control cabinet and the KEWA process control – the software the system uses to modify printing parameters such as flow rate, sheath gas, etc. A Velmex XY stage was used to control the motion as shown in Figure 2. The AJP used has the 300 µm nozzle tip and is capable of focusing an aerosol stream down to a tenth of the size of the nozzle orifice, resulting in 30 µm. Figure 3 shows some examples of narrow prints on different surface features – a 30 µm width printed line on a glass slide (a), a 400 µm deep silicon micromachined cavity (b), a 30 µm tall fragile spherical buckled polyimide structure (c) and a 1 mm carbon fiber rod (d). Clariant TPS 50G2 silver ink was used throughout all printing and the process recipes were optimized/tuned by changing the sheath flow rate, atomizer flow rate, substrate material, stand-off distance and stage speed to change the morphology of the printed lines.

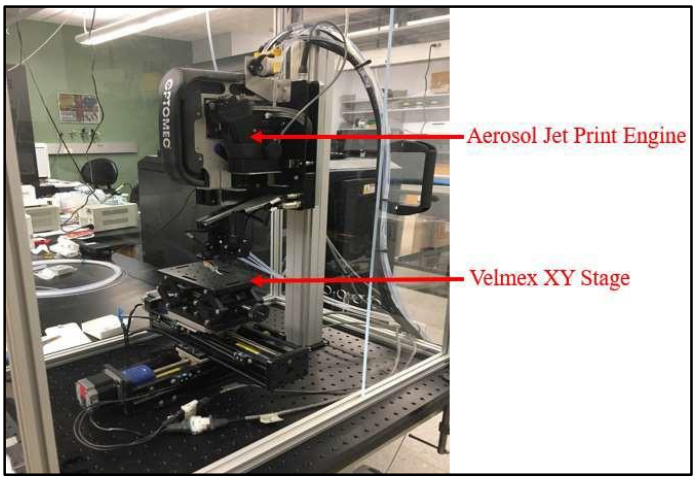

FIGURE 2: MOUNTED OPTOMEC AEROSOL PRINT ENGINE AND THE VELMEX XY STAGE.

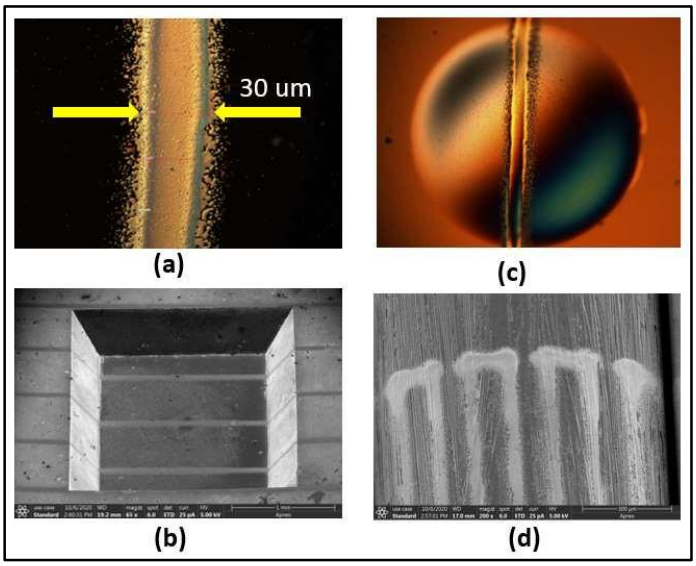

FIGURE 3: 30-MICRON SILVER LINES PRINTED ON (a) A GLASS SLIDE, (b) A 300 µm DEEP SILICON MICROMACHINED CAVITY, (c) A 30 µm TALL FRAGILE SPHERICAL BUCKLED POLYIMIDE DIAPHGRAM, (d) A 1 mm DIAMETER CARBON FIBER ROD.

2.2 Printing Process

For this experiment, the Optomec Decathlon engine was set to have a flow rate of 25 sccm, a sheath value of 30 sccm, and a divert and boost value of 50 sccm. The transducer was set to 500 mA and the Ultrasonic Atomizer bath was set to a temperature of 23 °C - close to room temperature. These

parameters were set using the KEWA process control software. The other parameters used that were set outside the KEWA software include setting the chiller to 15 °C and diluting the Clariant silver ink with deionized (DI) water. A ratio of 3:1 DI water to ink was used to lower the viscosity of the ink to the acceptable range – between 1-10 cP for the ultrasonic Decathlon print engine. These settings gave an average line width of 150 µm when examined under the microscope. The line width was always verified under the microscope before printing samples for the experiment to ensure consistency. All printing processes done in this study used these parameters and were printed at a speed of 5 mm/s. Once the print engine was tuned, 3x3mm Van der Pauw square pads were printed on a 2-inch glass slide using a shadow mask as shown in Figure 4. A shadow mask was used for this part of the research to improve the perimeter edge quality of the silver pads. A slightly overlapping serpentine structure was programmed to print the pads by adjusting the steps in the x-direction of the Velmex program to prevent any gaps. After printing, the Van der Pauw silver pads were sintered in the oven at a wide variety of times and temperatures.

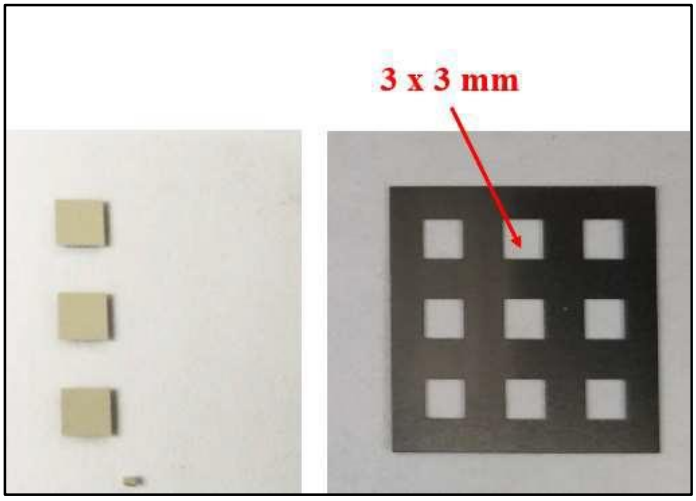

FIGURE 4: PRINTED SILVER PADS USING THE SHADOW MASK.

2.3 Sintering Process

Thermal curing using an oven is one of the most reliable curing approaches for nanoparticle inks. Initial heating of the printed features leads to the evaporation of the solvent, making the nanoparticles come in contact with each other. Further heating leads to fusion and causes the material to form a continuous layer. A temperature of approximately 300°C is typically required to remove most commonly used organic compounds completely [9]. However, some substrates – such as PCBs cannot be cured at high temperatures. If the curing temperature is not high enough to remove the solvents and the other organic compounds, it will lead to an increase in the electrical resistance of the printed devices [10]. Therefore, it is important to optimize the curing temperature along with the amount of time cured to reduce the electrical resistance of the printed material and improve the conductivity. In this study, a design of experiment (DOE) was developed to optimize the conductivity of the silver printed features on glass wafers using a Lindberg/Blue M oven as shown the in Figure 5.

FIGURE 5: LINDBERG/BLUE M OVEN USED FOR THERMAL CURING.

2.4 Conductivity Measurement

The DOE uses the Van Der Pauw Method to determine the conductivity [11]. This technique was established in 1958 and continues to be used to measure the resistivity of thin conducting films (film should be much thinner than its width or length). The Van Der Pauw method employs a four probes placed uniformly around the perimeter of the sample – two probes are used for the supply current, while the remaining two probes are used for voltage sensing as shown in Figure 6. According to the theory, resistivity can be calculated using Equation 1 and the conductivity of the material will be the inverse of the resistivity – calculated with Equation 2.

$$\rho = \frac{\pi}{\ln 2} h \frac{V_{AB}}{I_{AB}} = 5.44\, h \frac{V_{AB}}{I_{AB}} \quad (1)$$

Where h is the thickness of the film.

$$\sigma = \frac{1}{\rho} \quad (2)$$

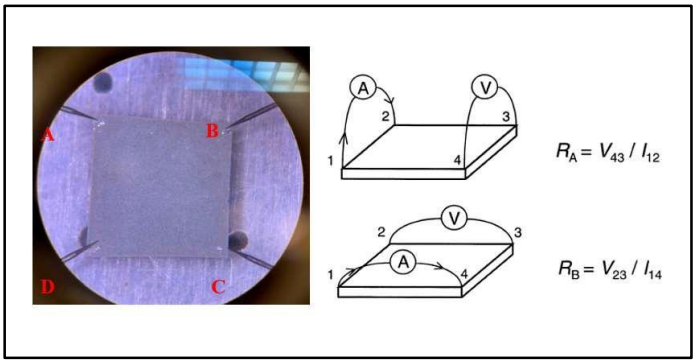

FIGURE 6: VAN DER PAUW MEASUREMENT TECHNIQUE FOR DETERMINING PAD RESISTIVITY.

A probe station equipped with 4 micromanipulator probes was used to determine the resistance by supplying 1 mA of current across adjacent pad corners, and then measuring the voltage in the opposing corners using a high-quality digital multimeter as shown in Figure 7. The sample was then rotated by 90 degrees and the process repeated until all combinations were measured. An average reading was then calculated. A Dektak profilometer was used to find the average thickness of the film.

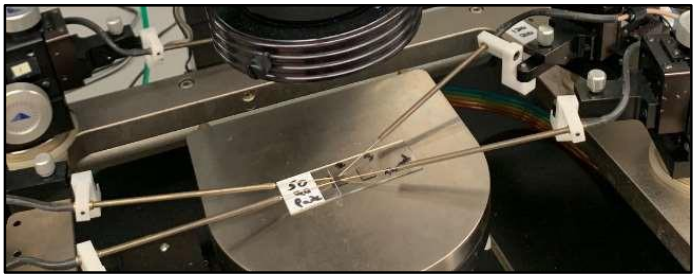

FIGURE 7: EXPERIMENTAL SETUP TO DETERMINE THE RESISTIVITY OF THE PRINTED SILVER PAD AFTER THERMAL CURING.

3. RESULTS AND DISCUSSION

As discussed in the previous section, the experiment was performed by sintering printed silver pads in an oven at a wide variety of combinations of time and temperature. The temperatures, in Celsius, used for the experiment were 120, 150, 200 and 250. For each temperature value, a sample was taken out at the following time values: 0.5, 1, 10, 20 and 40 hours. Resistivity was measured using the probe station and the average thickness of each pad was determined using the Dektak profilometer as shown in Figure 8. The roughness in the pad's top surface profile is due to the slight overlapping of lines in the serpentine structure. Each sample had three pads and the best two pads were selected out of the three to find the conductivity. The 40 trials were conducted in random order yielding the data in Table 1 below.

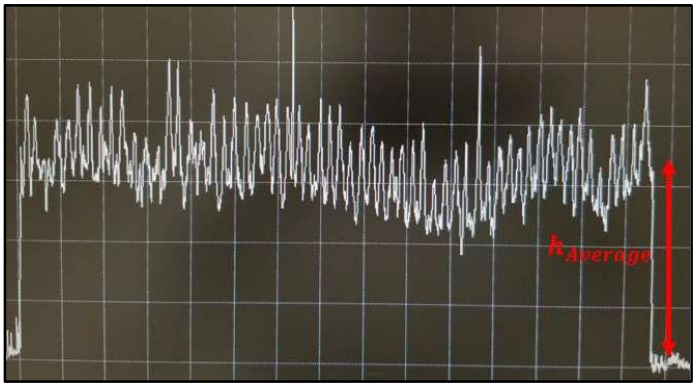

FIGURE 8: DEKTAK PROFILE OF A 3x3mm PAD.

TABLE 1: EXPERIMENTAL DATA FROM THE 40 RANDOMIZED PADS.

Run Order	Temperature (°C)	Curing Time (hrs)	Conductivity Response 1 (Ω^{-1} m^{-1})	Conductivity Response 2 (Ω^{-1} m^{-1})
1	120	0.5	NO RESPONSE	NO RESPONSE
2	120	1	NO RESPONSE	NO RESPONSE
3	120	10	NO RESPONSE	NO RESPONSE
4	120	20	1.73E+06	1.84E+06
5	120	40	3.14E+06	3.30E+06
6	150	0.5	NO RESPONSE	NO RESPONSE
7	150	1	NO RESPONSE	NO RESPONSE
8	150	10	6.69E+06	5.88E+06
9	150	20	5.07E+06	4.85E+06
10	150	40	7.55E+06	6.90E+06
11	200	0.5	1.58E+07	1.90E+07
12	200	1	2.09E+07	2.43E+07
13	200	10	2.66E+07	2.70E+07
14	200	20	2.83E+07	2.65E+07
15	200	40	3.12E+07	3.26E+07
16	250	0.5	1.93E+07	2.55E+07
17	250	1	2.03E+07	2.17E+07
18	250	10	3.68E+07	3.20E+07
19	250	20	3.81E+07	3.51E+07
20	250	40	4.61E+07	4.71E+07

Linear regression modelling reveals that both time (t) and temperature (T) are highly significant in predicting conductivity. Minitab output including the ANOVA and R-sq values are shown below in Figure 9. The resulting linear regression equation is found to be:

$$\sigma = -3.62e7 + (2.64e5)(T) + (2.94e5)(t) \quad (3)$$

where T is Temperature (°C) and t is time (hours)

Model Summary

S	R-sq	R-sq(adj)	R-sq(pred)
5093542	88.76%	88.15%	86.59%

Analysis of Variance

Source	DF	Adj SS	Adj MS	F-Value	P-Value
Regression	2	7.577E+15	3.788E+15	146.03	0.000
Temp (deg C)	1	6.829E+15	6.829E+15	263.25	0.000
Time (hrs)	1	7.472E+14	7.472E+14	28.80	0.000
Error	37	9.599E+14	2.594E+13		
Lack-of-Fit	17	9.090E+14	5.347E+13	21.01	0.000
Pure Error	20	5.090E+13	2.545E+12		
Total	39	8.537E+15			

FIGURE 9: MINITAB OUTPUT OF THE MODEL SUMMERY AND ANOVA.

The high adjusted R-squared value (88.15%) indicates that the model explains a very high percentage of the variation seen in the data. Values over 70% are typically considered to be acceptable. To check for model adequacy, we analyzed residuals from the model (actual data minus predicted value). We find the residuals to be normally distributed, as indicted by the linearity observed on the probability plot in Figure 10. We also see no discernable patterns in the residuals versus fits or in the residuals

versus run order which would indicate a problem in the model or experimental setup.

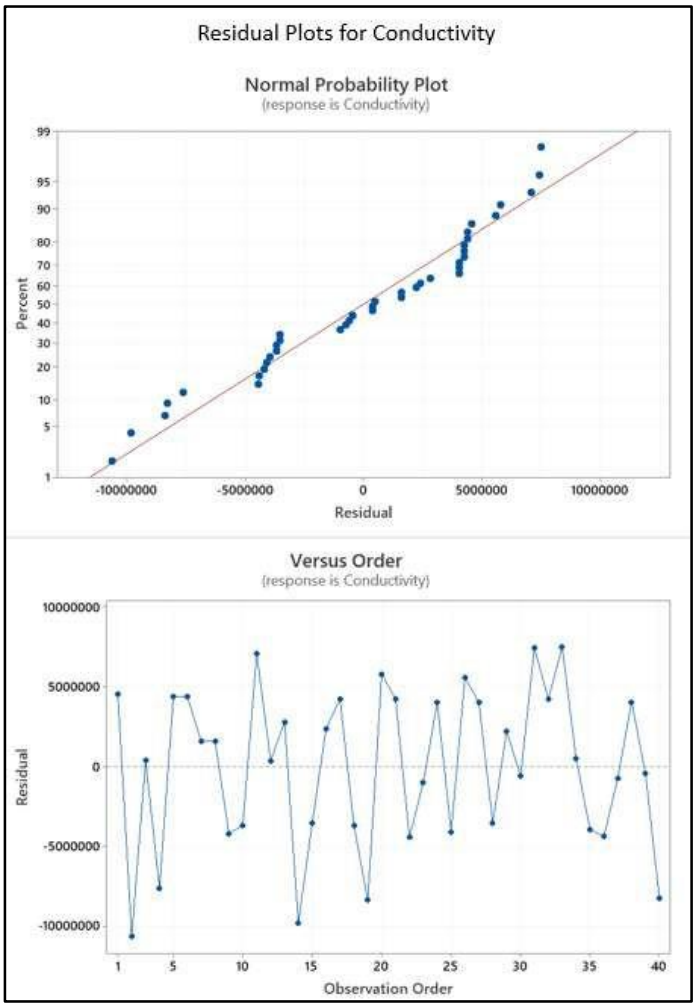

FIGURE 10: RESIDUAL ANALYSIS TO CHECK FOR MODEL ADEQUACY.

In general, we conclude that the model is adequate in predicting conductivity for values of time ranging from 0 to 40 hours and temperatures ranging from 120-250 ℃. A contour plot of conductivity versus time and temperature is shown in figure 11. This model can be used to predict the conductivity for certain time and temperature and benefitted to many applications.

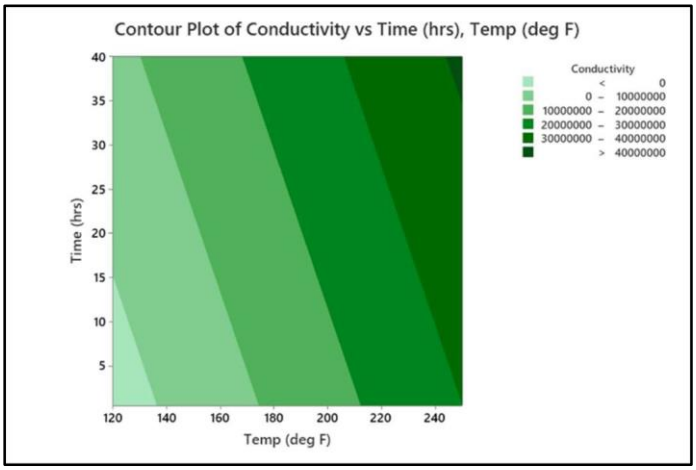

FIGURE 11: CONTOUR PLOT CONDUCTIVITY VERSUS TIME AND TEMPERATURE.

4. CONCLUSION

In summary, a design of experiment (DOE) was introduced to characterize the conductivity of aerosol jet printed silver features on glass substrates and to develop a reusable model for other printable materials. This study utilized an Optomec Decathlon print engine and Clariant Ag ink to print 3x3mm square pads on 2-inch glass wafers using a shadow mask. The samples were then cured using an oven with different time and temperature values. The Van der Pauw method was applied to determine the conductivity values for each pad and afterwards a linear regression model was developed to successfully predict the conductivity for time values ranging from 0 to 40 hours and temperatures ranging from 120-250 ℃ by analyzing the collected experimental data. Although only demonstrated with an oven and one type of ink, this procedure can be done with any material and any post processing method to develop an equation that can predict conductivity with a few given variables.

ACKNOWLEDGEMENTS

This research was supported by National Science Foundation Award ECCS- 2025075 which is part of the NSF National Nanotechnology Coordinated Infrastructure (NNCI) and National Science Foundation Award ECCS-1828355 which is a part of MRI (Development of a Multiscale Additive Manufacturing Instrument with Integrated 3D Printing and Robotic Assembly).

REFERENCES

[1] M. Maher, A. Smith, and J. Margiotta, A synopsis of the Defense Advanced Research Projects Agency (DARPA) investment in additive manufacture and what challenges remain (SPIE LASE). SPIE, 2014.

[2] N. J. Wilkinson, M. A. A. Smith, R. W. Kay, and R. A. Harris, "A review of aerosol jet printing—a non-traditional hybrid process for micro-manufacturing," The International Journal of Advanced Manufacturing

Technology, vol. 105, no. 11, pp. 4599-4619, 2019/12/01 2019, doi: 10.1007/s00170-019-03438-2.
[3] OPTOMEC, "AEROSOL JET PRINTED ELECTRONICS OVERVIEW."
[4] T. Rahman, L. Renaud, D. Heo, M. Renn, and R. Panat, "Aerosol based direct-write micro-additive fabrication method for sub-mm 3D metal-dielectric structures," Journal of Micromechanics and Microengineering, vol. 25, no. 10, p. 107002, 2015.
[5] K. K. Christenson, J. A. Paulsen, M. J. Renn, K. McDonald, and J. Bourassa, "Direct printing of circuit boards using Aerosol Jet®," in NIP & Digital Fabrication Conference, 2011, vol. 2011, no. 2: Society for Imaging Science and Technology, pp. 433-436.
[6] M. Hedges and A. B. Marin, "3D Aerosol jet printing-Adding electronics functionality to RP/RM," in DDMC 2012 conference, 2012, pp. 14-15.3.
[7] K. Schuetz, J. Hörber, and J. Franke, "Selective light sintering of Aerosol-Jet printed silver nanoparticle inks on polymer substrates," in AIP Conference Proceedings, 2014, vol. 1593, no. 1: American Institute of Physics, pp. 732-735.
[8] A. Shankar, E. Salcedo, A. Berndt, D. Choi, and J. E. Ryu, "Pulsed light sintering of silver nanoparticles for large deformation of printed stretchable electronics," Advanced Composites and Hybrid Materials, vol. 1, no. 1, pp. 193-198, 2018.
[9] A. Kamyshny, J. Steinke, and S. Magdassi, "Metal-based inkjet inks for printed electronics," The Open Applied Physics Journal, vol. 4, no. 1, 2011.
[10] L. Makkonen, "On the Methods To Determine Surface Energies," Langmuir, vol. 16, no. 20, pp. 7669-7672, 2000/10/01 2000, doi: 10.1021/la990815p.
[11] O. Philips'Gloeilampenfabrieken, "A method of measuring specific resistivity and Hall effect of discs of arbitrary shape," Philips Res. Rep, vol. 13, no. 1, pp. 1-9, 1958.